Journal of Inorganic and Organometallic Polymers and Materials (2022) 32:4373–4383
https://doi.org/10.1007/s10904-022-02424-8

Structural Engineering of ZnO–SnO_2–Ag(AgCl) Nanocomposites for the Medical Applications

S. K. Evstropiev[1,2,3] · A. V. Karavaeva[4] · N. V. Nikonorov[3] · V. N. Vasilyev[3] · A. S. Saratovskii[2]

Received: 24 April 2022 / Accepted: 18 June 2022 / Published online: 28 July 2022

Abstract
ZnO–SnO_2–Ag(AgCl) nanocomposites consisting of hexagonal ZnO, tetragonal SnO_2, metallic Ag and AgCl nanocrystals were prepared by wet polymer-salt synthesis. The materials were studied using optical and luminescent spectroscopy, SEM, EDS and XRD analysis. The ability to generate chemically active singlet oxygen and antibacterial activity of prepared materials against both gram-positive and gram-negative bacteria were tested. It was showed that Ag structural transformation starts in initial composite solutions and proceeds at all stages including drying and thermal treatment of ZnO–SnO_2–Ag(AgCl) synthesis. During this transformation, Ag exists in different forms (ions, molecular clusters, metallic and salt (AgCl) nanoparticles) and structural states (free Ag^+ ions and Ag-PVP complexes in the solutions; Ag^+ ions embedded into oxides crystal matrices; molecular clusters in the solutions and in PVP-salt composites; nanoparticles). Synthesized ZnO–SnO_2–Ag(AgCl) powders consist of small (about 50 nm) nanoparticles—"nanogenerators" of chemically active singlet oxygen. This provides high antibacterial activity of these materials against both gram-positive and gram-negative bacteria.

Keywords Nanoparticle · Spectroscopy · ZnO · Ag · Singlet oxygen · Bactericidal properties

1 Introduction

The development of new effective photocatalytic and bactericidal materials for medical and environmental applications is actual problem. Oxide photocatalytic and bactericidal materials are chemically durable, ecological, cheap and promising for wide practical applications [1–7].

It is known that the photogeneration of the chemically active oxygen is one of the main mechanisms in determining photocatalytic and bactericidal properties of oxide materials. The mechanisms of this phenomenon was studied and discussed in many works [4–9]. The effectiveness of this photogeneration depends on the characteristics of excited radiation and on the electronic structure and the morphology of oxide materials [6–11].

The formation of chemically active oxygen species occurs on the materials surface. So, the application of nanomaterials having high specific surface area provides significant enhancement of photocatalytic and bactericidal properties compared with macroscopic materials [12]. The values of specific area of material surfaces grow with a decrease in their particles sizes. It determines significant increase in the photocatalytic properties and antibacterial activity of highly disperse materials. The nanoparticles (NPs) forming chemically active oxygen under light irradiation are called "nanogenerators" which play a key role in the photocatalytic and bactericidal properties of oxide materials. Thus, the strategy of the new photoactive materials development should be focused on the study and optimization of these nanoparticles.

The hetero-structure consisting of two different closely packed oxide semiconductor NPs demonstrate significantly higher photocatalytic and bactericidal properties compare with single-component [13, 14]. This phenomenon is related to the spatial separation of photo-generated electrons and holes and the prevention of their recombination. Recombination processes strongly decrease the effectiveness of photo

✉ S. K. Evstropiev
evstropiev@bk.ru

1 SPA "Vavilov State Optical Institute, Saint-Petersburg, Russia

2 Saint-Petersburg State Technological Institute (Technical University), Saint-Petersburg, Russia

3 ITMO University, Saint-Petersburg, Russia

4 Saint-Petersburg State Chemical-Pharmaceutical University, Saint-Peterburg, Russia

excitation of materials and reduce their photocatalytic and bactericidal properties.

ZnO and ZnO-based nanocomposites containing SnO_2 or Ag additions have high photocatalytic and bactericidal properties and can be used in oncology [11–23]. Different nanomaterials containing ZnO NPs doped with silver compounds demonstrate high luminescent, photocatalytic and antibacterial properties and are very promising for different optical, environmental and medical applications [10, 23–30]. The plasmon-exciton interaction in these composites determines significant enhancement of their luminescence properties in near UV spectral range comparing with pure ZnO [24, 29–31]. It is worth noting that the structure, morphology and luminescence properties of ZnO-based nanocomposites doped with Ag significantly depend on the method of their preparation [24, 29–33].

Many different technological methods (electrospinning and subsequent calcination [25], liquid polymer-salt methods [30–33], sol–gel [34], hydrothermal synthesis [28], MOCVD [27], co-precipitation [35], ultrasonification [36]) have been applied for the synthesis of Ag-doped ZnO crystals.

Ag can be presents in different structural forms in ZnO-based nanocomposites depending on the method and technological conditions on their preparation. In [29] preliminary synthesis, Ag NPs were deposited on the surface of ZnO NPs for the formation of ZnO/Ag nanocomposites. Ag formed Ag_2O NPs on the surface of ZnO micro-flowers [37] or nanofibers [25] which were formed earlier in the solution. In ZnO/Ag nanocomposites synthesized in [38] by spray pyrolysis or solvothermal methods all Ag also present in the form of NPs. Contrary, in ZnO/Ag nanocomposites prepared by sol–gel synthesis some part of silver was embedded into ZnO crystal matrix [39]. Diffusion of Ag^+ ions into ZnO crystal matrix was discussed also in [40, 41]. Thus, the structural form of silver in ZnO/Ag nanocomposites depends on technological method used for their preparation and was discussed in many works.

The polymer-salt technique which involves the application of liquid film-forming solutions is simple, non-expensive and can be used for the preparation of different oxides [11, 18, 33, 42]. In this method, homogeneous and transparent solutions containing soluble polymer and thermally decomposable metal salts are used as oxide NPs precursors. The coated materials are subjected to drying followed by thermal treatment.

The aim of this work is focused on the polymer-salt synthesis of Ag-containing ZnO–SnO_2 nanocomposites, the study of Ag influence on their structure, spectral and luminescence properties, the ability to generate singlet oxygen under light irradiation and their antibacterial activity against gram-positive and gram-negative bacteria. New high effective photoactive and bactericidal materials with the defects-engineered structure and the simple and cheap method of its fabrication were the targets of this study.

2 Materials and Methods

Aqueous solutions of $Zn(NO_3)_2$, $SnCl_2$, $AgNO_3$ and high-molecular polyvinylpyrrolidone (Sigma Aldrich, $M_w = 1{,}300{,}000$ g/mol) were used for powders synthesis. These solutions were mixed together at room temperature with vigorous stirring for 1 h. Small particles of AgCl were formed in the solutions during their mixing. Drying of the resultant homogeneous liquid mixtures was performed by air at 20 °C. Thermal treatment of dried samples was carried out at atmospheric pressure at 550 °C for 2 h. Such thermal treatment provides full decomposition of metal nitrates and PVP [18]. Nominal chemical compositions of prepared solutions and calculated chemical compositions of the obtained powders are given in Table 1.

XRD and SEM analysis was carried out for the study of the structure and morphology of prepared materials. Chemical composition and materials morphology were studied

Table 1 Chemical composition of prepared materials

Sample	Chemical compositions of aqueous solutions, wt%					Calculated chemical compositions of powders, wt.%		
	H_2O	PVP	$Zn(NO_3)_2$	$SnCl_2$	$AgNO_3$	ZnO	SnO_2	Ag*
1	95.91	2.38	1.51	0.20	–	80.25	19.75	–
2	95.90	2.38	1.51	0.20	0.01	79.66	19.60	0.74
3	95.90	2.37	1.51	0.20	0.02	79.07	19.46	1.47
4	95.89	2.37	1.51	0.20	0.03	78.49	19.32	2.19
5	95.83	2.37	1.51	0.20	0.09	74.55	18.81	6.64
6	95.47	2.36	1.50	0.20	0.47	58.42	14.38	27.20
7	95.01	2.35	1.50	0.20	0.94	45.92	11.30	42.78
8	94.56	2.34	1.49	0.20	1.41	37.83	9.31	52.86
9	94.13	2.33	1.48	0.20	1.86	32.15	7.92	59.93

*All silver content in powders is taken into account in the form of metallic Ag

using microscope VEGA3 TESCAN with energo-dispersive analysis attachment Essence™ EDS.

The difference between nominal and analytical chemical compositions of prepared materials was < 5 wt%. The diffractometer Rigaku Ultima IV was used for XRD analysis of prepared materials. The diffraction patterns were scanned from 20° to 65° (2θ). UnitCell software was used to refine the unit cell parameters of prepared powders [43].

The measurements of materials luminescence spectra (λ_{ex} = 370 nm) in visible spectral range (400–700 nm) were carried out using fluorescence spectrometer Perkin Elmer LS-50B. Double beam UV–Vis spectrophotometer Perkin-Elmer Lambda 650 was used for the measurements of absorption spectra.

It is known [6, 7] that chemically active singlet oxygen has characteristic luminescence band in NIR spectral diapason (λ_{max} = 1270 nm). Photoluminescence spectra in NIR spectral range was obtained upon the excitation with two different HPR40E LEDs (emission band maximum at λ_{max} = 370 nm; power density 0.35 W/cm^2) and (λ_{max} = 405 nm; power density 0.90 W/cm^2).

The method described in [44] was used for the estimation of bactericidal properties of prepared coatings. The experiments were carried out at natural lighting conditions. The representatives of gram-positive bacteria ***Staphylococcus aureus ATCC 209P*** and gram-negative bacteria ***Escherichia coli ATCC 25922*** were used as test bacteria. Bactericidal activity at room temperature was estimated by the measurement of the size of inhibited area, which is formed on surface containing bacteria. In the experiments, three samples of each powder were used and the test results were subsequently averaged.

3 Experimental Results and Discussion

Figure 1a presents absorption spectra of fresh solutions ***1–4***. Some bend at λ = 300–305 nm related to the absorption band of nitrate anions [45] is observed in absorption spectrum of solution ***1***. It is worth to notice that small $AgNO_3$ additions into the solutions significantly increase absorption in UV spectral diapason and shift absorption edge into the longer wavelengths. It is worth to notice that the addition of even small amounts of $AgNO_3$ into the solution leads to a significant increase of light absorption in UV spectral range (curves 2–4, Fig. 1a). The slight difference in chemical compositions between solutions ***1*** (curve 1) and solutions ***2–4*** (curves 2–4) cannot explained the observed difference in absorption spectra. It is possible to suggest that this phenomenon related to the fast formation of small molecular clusters Ag_n in these solutions. It is known [32, 33, 46–50] that such clusters have intensive absorption bands in UV spectral range. The comparison of

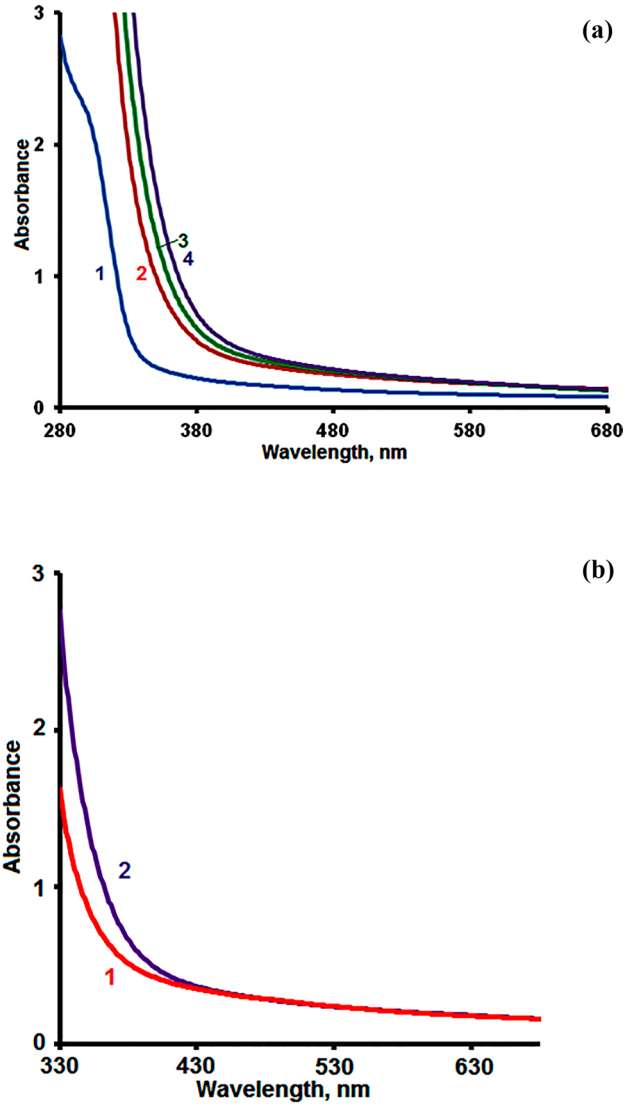

Fig. 1 **a** Absorption spectra of as-prepared solutions ***1*** (curve 1), ***2*** (curve 2), ***3*** (curve 3), ***4*** (curve 4). **b** Absorption spectra of as-prepared solution 2 (curve 1) and after the storage during 7 days (curve 2)

absorption spectra of the solutions 2–4 (curves 2–4) shows that the increase of $AgNO_3$ content (Table 1) leads to the growth of the amount of these silver clusters and shifts absorption edge into the longer wavelength diapason.

Characteristic plasmonic absorption band of silver NPs is absent in the solutions absorption spectra presented in Fig. 1a. This is related to the small $AgNO_3$ content in solutions 1–4 (Table 1). Usually, the presence of this Ag plasmonic band in absorption spectra is the result of intensive reduction of silver ions and this band is shown often in the spectra of the solutions with high Ag content or subjected light irradiation [32, 33]. Spectral position of this band depends on the concentration of Ag NPs.

The transformation of Ag structural forms is significantly accelerated under light irradiation even at the presence of stabilizing additives [33]. However, some changes in the absorption spectra of our solutions are observed also after the storage in the darkness (Fig. 1b). This phenomenon is explained by the presence of PVP in solutions compositions (Table 1). Besides stabilization effect [51, 52], PVP in the solution can reduce Ag^+ ions [53]. This reduction of Ag^+ ions leads to the formation of an additional amount of silver clusters having absorption bands in UV spectral range. This phenomenon is responsible for the spectral changes in prepared solutions during their storage in the darkness.

The study of photoluminescence spectra in visible spectral range of prepared solutions confirms the formation of small silver molecular clusters. The intensity and spectral positions of luminescence bands of these clusters depend on their electrical charge + 1 or neutral clusters and the amounts of Ag atoms in the materials structure [48, 50, 54]. The photoluminescence spectra of solution ***4*** (Table 1) at different excitation wavelengths are shown in Fig. 2a. The luminescence bands with λ_{max} ~ 490 nm and ~ 605 nm, described previously in [32, 33, 46, 48, 50] are seen in these spectra. According to [32, 33, 48, 50] the main input in the luminescence at 605 nm can be related to the presence of Ag_2, Ag_4, Ag_{+4} and Ag_5 clusters.

Figure 3 shows SEM images at different magnification of the samples ***4*** (a,b) and ***5*** (c,d). It is seen that the samples contain grains with different shape and size which varies from 5 up to 20 µm. The application of high magnification (Fig. 3b, d) shows that these grains are not monolithic and have the structure consisting of small nanoparticles having size 50–60 nm. Such morphology provides high specific surface area that promotes high photocatalytic and bactericidal properties of the materials. The similar photos were observed for all prepared samples and the significant influence of Ag content on materials morphology was absent.

The data of energy-dispersive analysis of powder ***5*** are presented in Fig. 4. The peaks of main components (Zn, Sn, Ag, O) of prepared materials (Table 1) are observed in this diagram. The experimental data obtained by the EDS method showed consistency with the experimental and calculated chemical compositions of the synthesized powders.

XRD patterns of prepared powders with different Ag content (powders ***4*** and ***8***) are given in Fig. 5. Numerous peaks attributed to hexagonal ZnO crystals (JCPDS card No. 36-1451) and tetragonal SnO_2 crystals (JCPDS card No. 41-1445), metallic Ag (JCPDS card No. 04-0783) and face-centered cubic (chlorargyrite) phase (reference JCPDS Card No. 31-1238) of the AgCl are observed in these patterns. The peaks of ZnO crystals are the most intense and the ratio between the intensities of these peaks is close to the standard data (JCPDS card No. 36-1451).

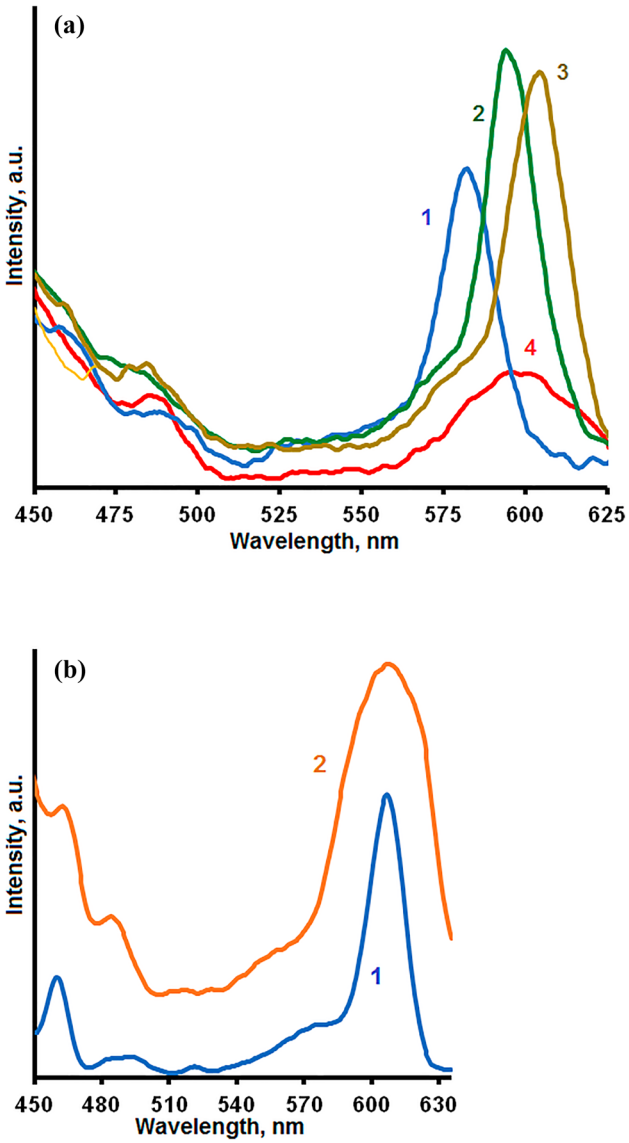

Fig. 2 **a** Photoluminescence spectra of solution ***4***. Excitation wavelength, nm: 390 (curve 1); 400 (curve 2); 405 (curve 3); 410 (curve 4). **b** Photoluminescence spectra of composite coating prepared from solution ***4***. Excitation wavelength, nm: 405 (curve 1); 415 (curve 2)

Significant growth of the intensities of AgCl and Ag peaks is observed with the increase in Ag content. The simultaneous presence of various forms of silver in powders can be associated with a complex transformation of its structural state during heat treatment in air atmosphere.

The influence of Ag doping on the crystallization mechanism of ZnO crystals and their structures was studied earlier in [25, 27, 34, 39, 40]. So, authors [34] reported that doping ZnO with Ag during sol–gel synthesis reduces the average ZnO crystal size.

Based on obtained XRD data it is possible to suggest that Ag ions penetrate inside the growing ZnO and SnO_2 crystals and modified their structure increasing lattice parameters

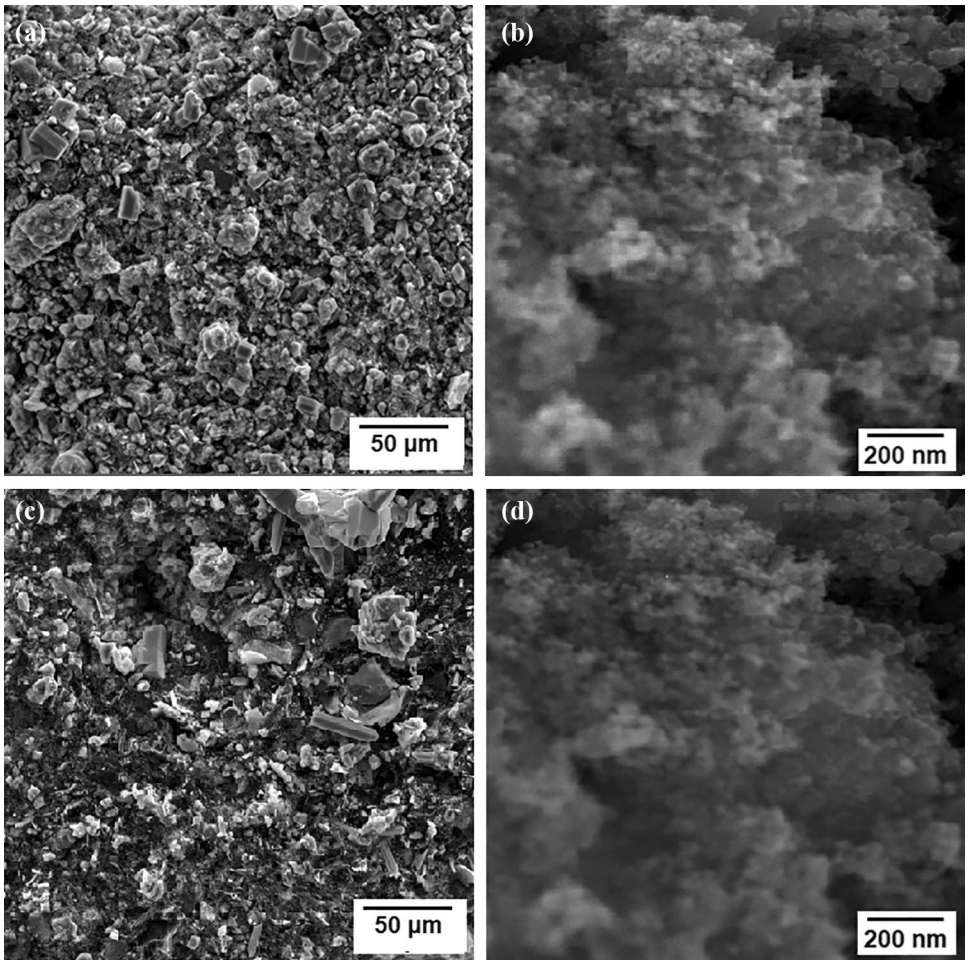

Fig. 3 SEM images of prepared powders ***4*** (**a**, **b**) и ***5*** (**c**, **d**) (Table.1)

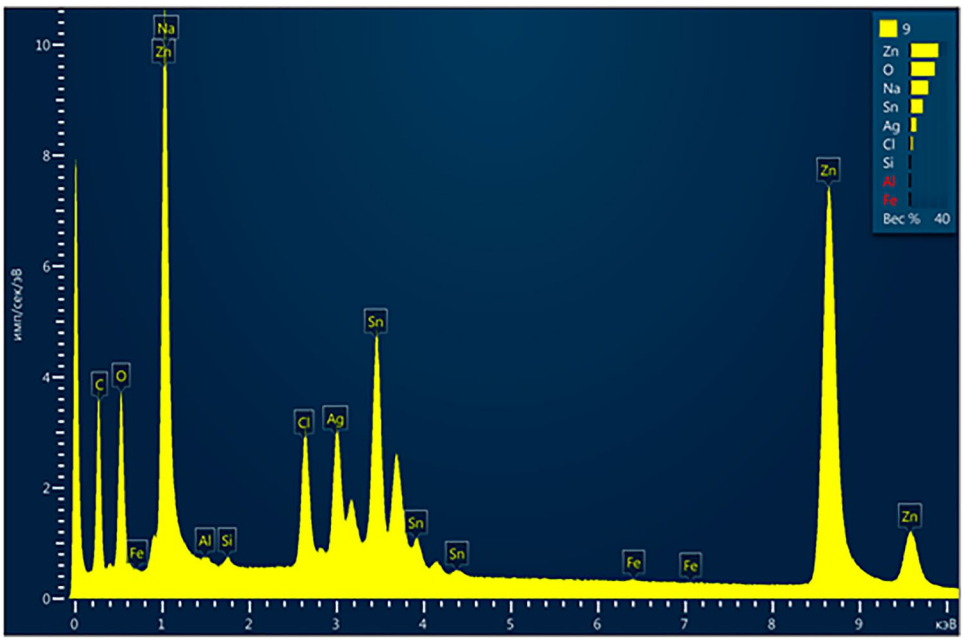

Fig. 4 The data of EDS analysis of powder ***5***

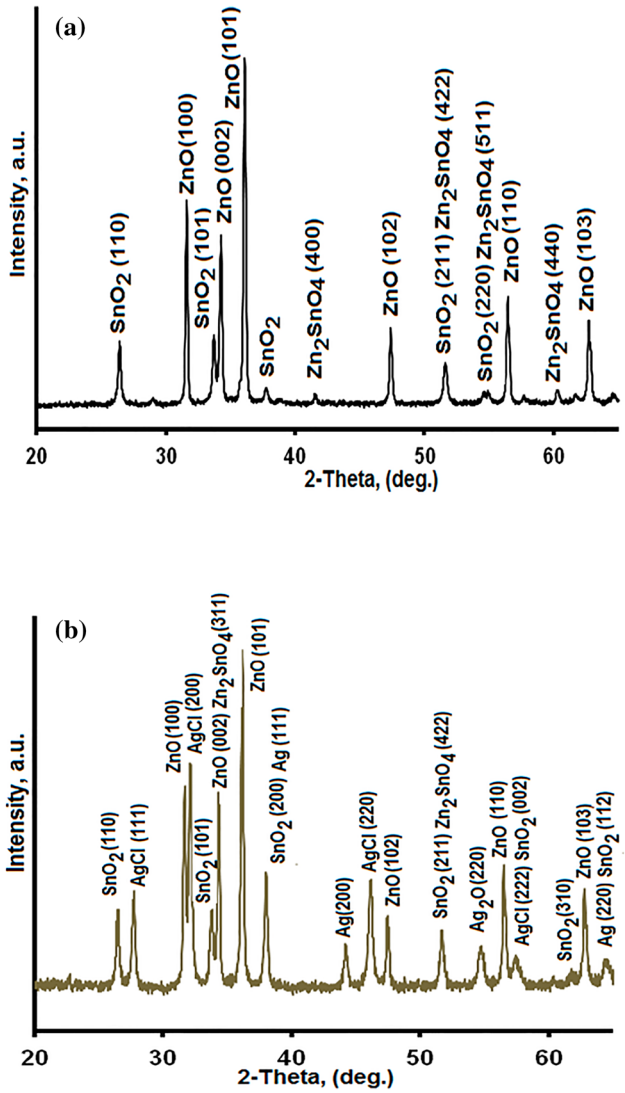

Fig. 5 XRD patterns of the powders ***1*** and ***9*** with different Ag content

(Tables 2, 3). Similar results were observed previously in [39] for Ag-doped ZnO nanoparticles prepared by sol–gel method. The possibility of Ag^+ diffusion from Ag_2O powder into ZnO crystal matrix during thermal treatment at 200–250 °C was discussed also in [40]. The incorporation of Ag^+ ions into the ZnO lattice through substitution of Zn^{2+} ions is difficult due to their higher ionic radius 1.22 Å in comparison with the radius of Zn^{2+} ions 0.74 Å [41].

Figure 6 demonstrates the dependence of the cell volumes of ZnO (a) and SnO_2 (b) crystals from Ag content in prepared ZnO–SnO_2–Ag(AgCl) materials. It is seen that the growth of Ag content leads to a significant cell expansion of both crystal oxides. The change of the parameters of the crystal cell at the incorporation of the doping component is well-known phenomenon. Such variations of ZnO crystal cell parameters at Gd doping were described previously in [55].

Observable ZnO and SnO_2 crystal cells expansion in our samples can be related to the some features of polymer-salt synthesis. Our initial compositions included the mixtures of PVP and metal nitrates which were decomposed simultaneously with heat realization at 300–500 °C and formed oxides crystals [18] and Ag during the thermal treatment. So, the incorporation of Ag into ZnO and SnO_2 matrices can be attributed to initial stages of their crystals formation and growth.

Besides the crystal cells distortion, Ag diffusion into ZnO and SnO_2 crystals leads to the formation of structural defects in the crystals structures. Figure 7 demonstrates photoluminescence spectra of prepared powders in visible spectral range. The most intense peaks attributed to ZnO crystals [39, 41] defects are observed at 450 nm and 485 nm. Similar peaks of photoluminescence spectra of ZnO:Ag materials in this spectral region was observed previously in [31, 39, 41]. The observed intensive luminescence in visible spectral range indicates the high concentrations of structural defects in obtained nanocomposites. Taking in account the

Table 2 Lattice parameters of ZnO crystals in ZnO–SnO_2–Ag(AgCl) materials

Sample	Crystal lattice parameters			
	a, Å	c, Å	c/a	V, Å^3
1	3.2507 ± 0.0004	5.2069 ± 0.0008	1.6018	47.65 ± 0.01
2	3.2507 ± 0.0003	5.2091 ± 0.0012	1.6021	47.67 ± 0.02
3	3.2516 ± 0.0004	5.2085 ± 0.0009	1.6018	47.69 ± 0.02
4	3.2523 ± 0.0006	5.2105 ± 0.0012	1.6021	47.73 ± 0.02
6	3.2516 ± 0.0005	5.2095 ± 0.0012	1.6021	47.70 ± 0.01
7	3.2543 ± 0.0008	5.2118 ± 0.0016	1.6015	47.80 ± 0.02
8	3.2542 ± 0.0016	5.2187 ± 0.0032	1.6037	47.86 ± 0.05
9	3.2557 ± 0.0011	5.2170 ± 0.0023	1.6024	47.89 ± 0.03
JCPDS	3.2500	5.2070	1.6020	47.63
ZnO nanocrystals prepared by precipitation method in [58]	3.2547	5.2158	1.6025	47.85

Table 3 Lattice parameters of SnO_2 crystals in ZnO–SnO_2–Ag(AgCl) materials

Sample	Crystal lattice parameters			
	a, Å	b, Å	c, Å	V, Å^3
1	4.7370 ± 0.0009	4.7370 ± 0.0009	3.1855 ± 0.0007	71.48 ± 0.03
2	4.7399 ± 0.0011	4.7399 ± 0.0011	3.1858 ± 0.0009	71.58 ± 0.02
3	4.7412 ± 0.0003	4.7412 ± 0.0003	3.1868 ± 0.0002	71.64 ± 0.01
4	4.7459 ± 0.0007	4.7459 ± 0.0007	3.1866 ± 0.0006	71.77 ± 0.02
6	4.7412 ± 0.0013	4.7412 ± 0.0013	3.1872 ± 0.0012	71.64 ± 0.04
7	4.7433 ± 0.0009	4.7433 ± 0.0009	3.2045 ± 0.0012	72.10 ± 0.04
8	4.7466 ± 0.0023	4.7466 ± 0.0023	3.2058 ± 0.0020	72.23 ± 0.07
9	4.7479 ± 0.0022	4.7479 ± 0.0022	3.2049 ± 0.0022	72.25 ± 0.09
SnO_2 crystals	4.7391	4.7391	3.1869	71.5748

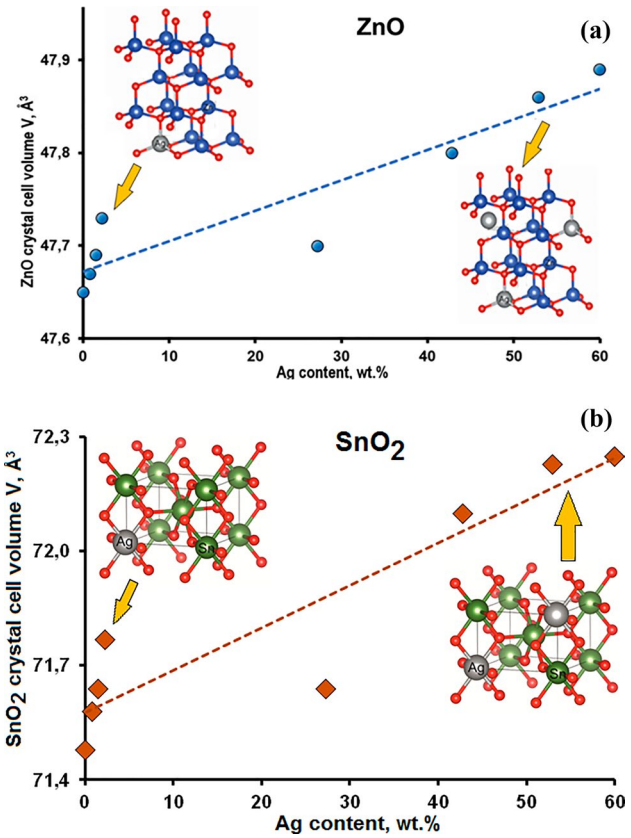

Fig. 6 The dependences of the crystals cells volumes of ZnO (**a**) and SnO_2 (**b**) crystals from the contents of Ag_2O in prepared powders

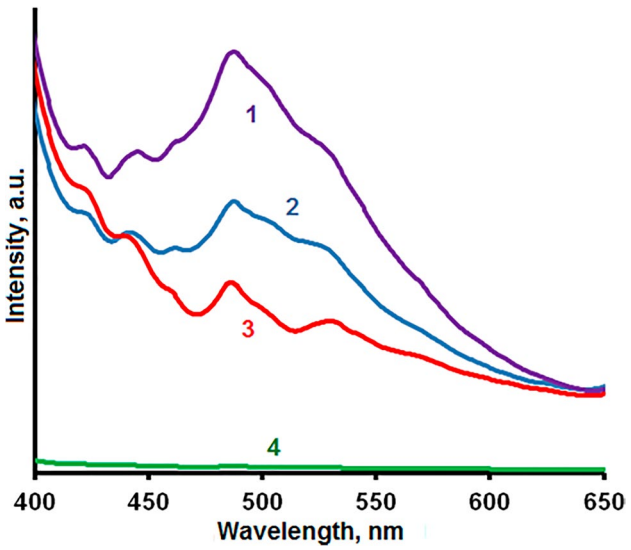

Fig. 7 Photoluminescence spectra ($\lambda_{ex} = 370$ nm) of the powders 1 (curve 1); 3 (curve 2); 4 (curve 3); 6 (curve 4) in visible spectral range

significant role of such defects in the enhancement of photocatalytic properties and antibacterial activity of oxide semiconductors [56–58], these results are important.

It is worth noting that even small Ag additions change significantly the luminescence intensity in visible spectral range and spectra shape. This agrees with the data reported in [41]. The addition of the big amount of Ag to the materials composition leads to the remarkable (more than 20 times) decrease of luminescence intensity (curve 4, Fig. 7). This phenomenon is related to the formation and growth of metallic silver nanoparticles in the materials with high silver contents. Metallic silver nanoparticles have strong absorption band in visible spectral range [23, 33] that determines the drastic reduction in the materials luminescence intensity with addition of Ag content.

The measurements of the photoluminescence in NIR spectral region showed that prepared powders generated the singlet oxygen under UV (370 nm) and blue (405 nm) light irradiation. Figure 8 shows photoluminescence spectra of the powders ***5*** (Fig. 8a, c) and ***1*** (Fig. 8b). The luminescence band of singlet oxygen with a maximum $\lambda_{max} = 1270$ nm, which is characteristic of the $^1\Delta_g - {}^3\Sigma_g$ electronic transition [6, 7] are observed in these spectra. A slightly lower intensity of the singlet oxygen luminescence band is observed upon excitation by UV radiation ($\lambda_{ex} = 370$ nm), compared with the use of blue light

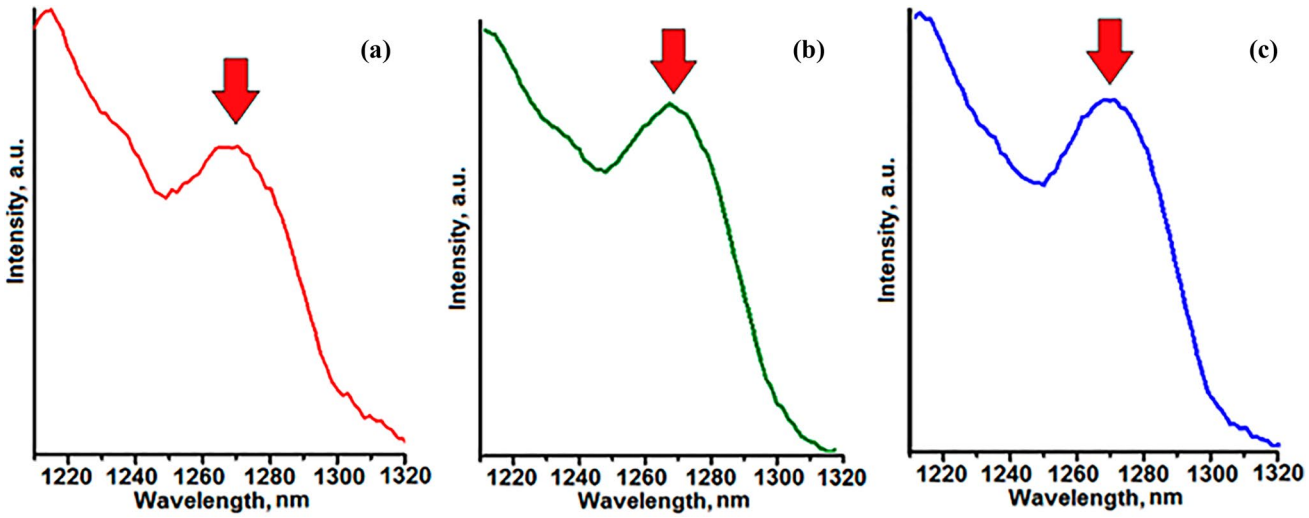

Fig. 8 Photoluminescence spectra ($\lambda_{ex} = 370$ nm) (**a**); $\lambda_{ex} = 370$ nm) (**b**, **c**) of the powders ***5*** (**a**, **c**) and ***1*** (**b**)

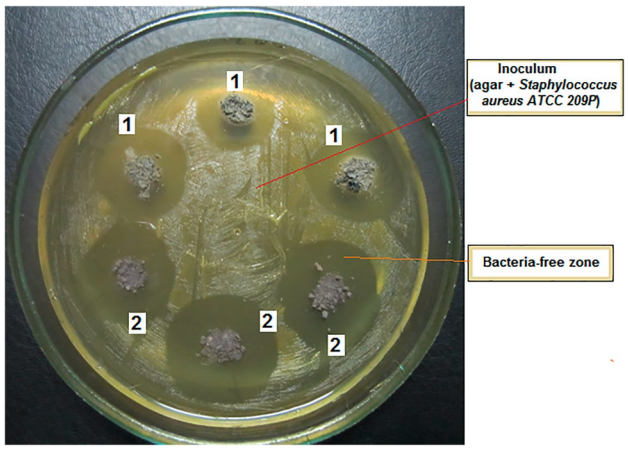

Fig. 9 Photo of ZnO-SnO_2-Ag(AgCl) powders ***3*** (samples 1) and ***4*** (samples 2) in Petri dish with the inoculums containing bacteria ***Staphylococcus aureus ATCC 209P***

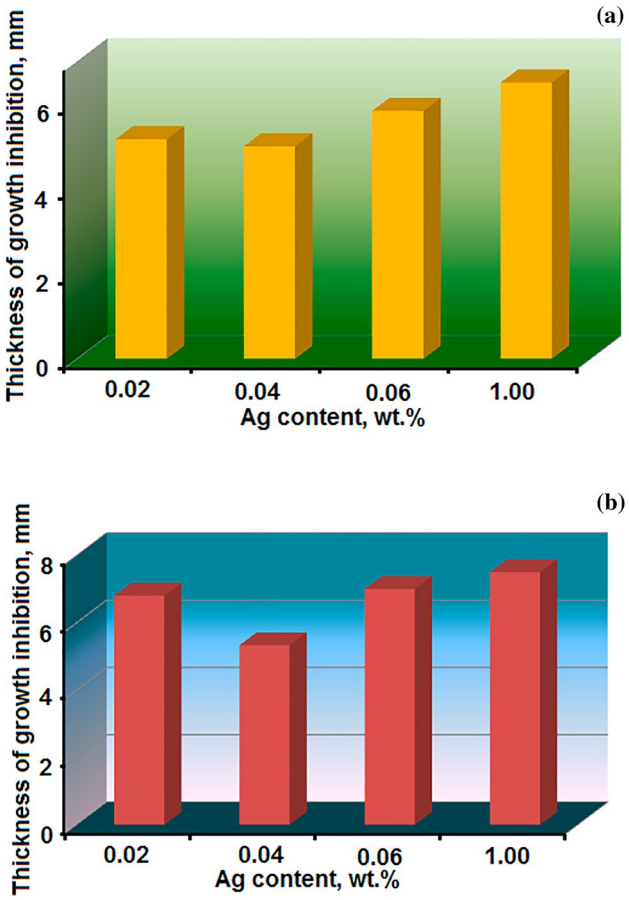

Fig. 10 Diagrams illustrating the influence of Ag content in prepared powders on their antibacterial activities against ***Staphylococcus aureus ATCC 209P*** (**a**) and ***Escherichia coli ATCC 25922***

($\lambda_{ex} = 405$ nm), which is associated with the lower power of the UV LED used (see above).

The experiments showed high antibacterial activity of prepared powders against both gram-positive and gram-negative bacteria. Figure 9 demonstrates the photo of ZnO–SnO_2-Ag(AgCl) powders ***3*** (samples 1) and ***4*** (samples 2) in Petri dish with the inoculums containing bacteria ***Staphylococcus aureus ATCC 209P***. Bacteria-free zones around all samples are seen in this photo. The comparison of size of these zones around powder 4 (samples 2, Fig. 9) with higher Ag content is somewhat bigger.

Figure 10 shows diagrams illustrating the influence of Ag content in prepared powders on their antibacterial activities against ***Staphylococcus aureus ATCC 209P*** (a) and ***Escherichia coli ATCC 25922*** (b). The increase of Ag content

enhances the antibacterial activity of prepared powders against both gram-positive and gram-negative bacteria. Although the high bactericidal properties of silver are well known, in our materials some part of Ag is inside oxide crystals and observed their high antibacterial activity was not obvious.

4 Conclusion

ZnO–SnO_2–Ag(AgCl) powders consisting of hexagonal ZnO, tetragonal SnO_2 nanocrystals, metallic Ag and AgCl crystals were prepared by wet polymer-salt synthesis. Ag additions into ZnO–SnO_2 materials significantly change their crystal structure, spectral, and luminescence properties.

Our experiments showed that Ag structural evolution starts in initial composite solutions and proceeds at all stages (drying, thermal treatment) of ZnO–SnO_2–Ag(AgCl) material synthesis. During this transformation, Ag exists in different forms (ions, molecular clusters, metallic and salt (AgCl) nanoparticles) and structural forms (free Ag^+ ions and Ag-PVP complexes in the solutions; Ag^+ ions embedded into oxides crystal matrices; molecular clusters in the solutions and in PVP-salt composites; nanoparticles).

Silver content has a significant impact on these Ag structural forms and also on the oxides (ZnO; SnO_2) crystal structure and luminescence properties of ZnO–SnO_2–Ag(AgCl) nanocomposites. These nanocomposites demonstrate that the photoluminescence in a visible spectral range is related to different defects of ZnO crystal structure. The addition of even a small amount of Ag significantly changes the luminescence intensity and spectra shape.

Obtained ZnO–SnO_2–Ag(AgCl) powders consist of small (about 50 nm) nanoparticles – "nanogenerators" of chemically active singlet oxygen. This is provides high antibacterial activity against both gram-positive and gram-negative bacteria.

Acknowledgements The work was funded by Russian Scientific Foundation (Grant No. 20-19-00559).

Funding Funding was provided by Russian Scientific Fund (20-19-00559).

Declarations

Conflict of interest The authors declare that they have no conflict of interest.

References

1. C.B. Ong, L.Y. Ng, A.W. Mohammad, A review of ZnO nanoparticles as solar photocatalysts: synthesis, mechanisms and applications. Renew. Sustain. Energy Rev. **81**(1), 536–551 (2018)
2. K.M. Lee, W. Lai, K.S. Ngai, C.J. Juan, Recent development of zinc oxide based photocatalyst in water treatment technology: a review. Water Res. **88**, 428–448 (2016)
3. K. Qi, B. Cheng, J. Yu, W. Ho, Review on the improvement of the photocatalytic and antibacterial activities of ZnO. J. Alloys Compd. **727**, 792–820 (2017)
4. F.X. Gamelin, G. Baquet, S. Berthoin, D. Thevenet, C. Nourry, S. Nottin, L. Bosquet, Effect of high intensity intermittent training on heart rate variability in prepubescent children. Eur. J. Appl. Physiol. **105**, 731–738 (2009). https://doi.org/10.1007/s00421-008-0955-
5. Y. Li, W. Zhang, J. Niu, Y. Chen, Mechanism of photogenerated reactive oxygen species and correlation with the antibacterial properties of engineered metal-oxide nanoparticles. ACS Nano **6**, 5164–5173 (2012)
6. D. Toshihiro, N. Yoshio, Formation and behavior of singlet molecular oxygen in TiO_2 photocatalysis studied by detection of near-infrared phosphorescence. J. Phys. Chem. C **111**, 4420–4424 (2007)
7. A.A. Krasnovsky, R.V. Ambartzumian, Tetracene oxygenation caused by infrared excitation of molecular oxygen in air-saturated solutions: the photoreaction action spectrum and spectroscopic parameters of the $^1\Delta_g \leftarrow {}^3\Sigma_g^-$ transition in oxygen molecules. Chem. Phys. Lett. **400**, 531–535 (2004)
8. F. Vatansever, W.C.M.A. de Melo, P. Avci, D. Vecchio, M. Sadasivam, A. Gupta, R. Chandran, M. Karimi, N.A. Parizotto, R. Yin, G.P. Tegos, M.R. Hamblin, Antimicrobial strategy centered around reactive oxygen species: bactericidal antibiotics, photodynamic therapy, and beyond. FEMS Microbiol. Rev. **37**, 955–989 (2013)
9. N. Akram, J. Guo, W. Ma, Y. Guo, A. Hassan, J. Wang, Synergistic catalysis of $Co(OH)_2$/CuO for the degradation of organic pollutant under visible light irradiation. Sci. Rep. **10**, 1019 (2020)
10. S. Das, A.J. Misra, A.P.H. Rahman, B. Das, R. Jayabalan, A.J. Tamhankar, A. Mishra, C.S. Lundborg, S.K. Tripathy, Ag@SnO2@ZnO core-shell nanocomposites assisted solar-photocatalysis downregulates multidrug resistance in Bacillus sp.: a catalytic approach to impede antibiotic resistance. Appl. Catal. B: Environ. **259**, 118065 (2019)
11. S.K. Evstrop'ev, V.M. Volynkin, V.M. Kiselev, K.V. Dukelskii, K.S. Evstrop'ev, V.V. Demidov, Y.A. Gatchin, Photocatalytic transparent coatings on the surface of the tips of medical fibre-optic bundles. Quantum Electron. **47**, 1125–1127 (2017)
12. K.R. Raghupathi, R.T. Koodali, A.C. Manna, Size-dependent bacterial growth inhibition and mechanism of antibacterial activity of zinc oxide nanoparticles. Langmuir **27**, 4040–4028 (2011)
13. S.K. Evstropiev, A.V. Karavaeva, M.A. Petrova, N.V. Nikonorov, V.N. Vasilyev, L.L. Lesnykh, K.V. Dukelskii, Antibacterial effect of nanostructured ZnO-SnO_2 coatings: the role of microstructure. Mater. Today Commun. **21**, 100628 (2019)
14. F. Lin, B. Cojocaru, C.L. Chou, C.A. Cadigan, Y. Ji, D. Nordlund, T.C. Weng, Z. Zheng, V.I. Pârvulescu, R.M. Richards, Photocatalytic activity and selectivity of ZnO materials in the decomposition of organic compounds. ChemCatChem **5**, 3841–3846 (2013)
15. S. Wang, P. Kuang, B. Cheng, J. Yu, C. Jiang, ZnO hierarchical microsphere for enhanced photocatalytic activity. J. Alloys Compds. **741**, 622–632 (2018)
16. Y. Wang, Q. Ma, H. Jia, Z. Wang, One-step solution synthesis and formation mechanism of flower-like ZnO and its structural and optical characterization. Ceram. Int. **42**, 10751–10757 (2016)
17. N. Vela, M. Calín, M.J. Yáñez-Gascón, I. Garrido, G. Pérez-Lucas, J. Fenoll, S. Navarro, Photocatalytic oxidation of six endocrine disruptor chemicals in wastewater using ZnO at pilot plant scale under natural sunlight. Environ. Sci. Pollut. Res. **25**, 34995–35007 (2018). https://doi.org/10.1007/s11356-018-1716-9
18. S.K. Evstropiev, L.L. Lesnykh, A.V. Karavaeva, N.V. Nikonorov, K.V. Oreshkina, L.Y. Mironov, S.Y. Maslennikov, E.V. Kolobkova, I.V. Bagrov, Intensification of photodecomposition of organics contaminations by nanostructured ZnO-SnO_2 coatings

prepared by polymer-salt method. Chem. Eng. Process. **142**, 107587 (2019). https://doi.org/10.1016/j.cep.2019.107587
19. R. Lamba, A. Umar, S.K. Mehta, S.K. Kansal, ZnO doped SnO_2 nanoparticles heterojunction photocatalyst for environmental remediation. J. Alloys Compds. **653**, 327–333 (2015)
20. P. Pascariu, A. Airinei, N. Olaru, L. Olaru, V. Nica, Photocatalytic degradation of Rhodamine B dye using ZnO-SnO_2 electrospun ceramic nanofibers. Ceram. Int. **42**, 6775–6781 (2016)
21. C. Wang, X. Wang, B.Q. Xu, J. Zhao, B. Mai, P. Peng, G. Sheng, J. Fu, Enhanced photocatalytic performance of nanosized coupled ZnO/SnO_2 photocatalytysts for methyl orange degradation. J. Photochem. Photobiol. A: Chem. **168**, 47–52 (2004)
22. H. Zhang, B. Chen, H. Jiang, C. Wang, H. Wang, X. Wang, A strategy for ZnO nanorod mediated multi-mode cancer treatment. Biomaterials **32**, 1906–1914 (2011)
23. S. Arooj, S. Nasir, A. Nadman, N. Ahmad, B. Muhammad, I. Ahmad, K. Mazhar, R. Abbasi, Novel ZnO: Ag nanocomposites induce significant oxidate stress in human fibroplast malignant melanoma (HT 144) cells. Beilstein J. Nanotechnol. **6**, 570–582 (2015)
24. B.J. Lawrie, R.F. Haglund Jr., R. Mu, Enhancement of ZnO photoluminescence by localized and propagating surface plasmons. Opt. Express **17**, 2565–2572 (2009)
25. Z. Cheng, S. Zhao, L. Han, A novel preparation method for ZnO/γ-Al_2O_3 nanofibres with enhanced absorbability and improved photocatalytic water-treatment performance by Ag nanoparticles. Nanoscale **10**, 6892–6899 (2018)
26. L. Xu, J. Miao, Y. Chen, J. Su, M. Yang, L. Zhang, L. Zhao, S. Ding, Characterization of Ag-doped ZnO film for its potential applications in optoelectronic devices. Optik **170**, 484–491 (2018)
27. A. Ievtushenko, V. Karpyna, J. Eriksson, I. Tsiaoussis, I. Shtepliuk, G. Lashkarev, R. Yakimova, V. Khranovskyy, Effect of Ag doping on the structural, electrical and optical properties of ZnO grown by MOCVD at different substrate temperatures. Superlattices Microstruct. **117**, 121–131 (2018)
28. Y. Zheng, L. Zheng, Y. Zhan, X. Lin, Q. Zheng, K. Wei, Ag/ZnO heterostructure nanocrystals: synthesis, characterization, and photocatalysis. Inorg. Chem. **46**, 6980–6986 (2007)
29. E.J. Guidelli, O. Baffa, D.P. Clarke, Enhanced UV emission from silver/ZnO core-shell nanoparticles: photoluminescence, radioluminescence, and optically stimulated luminescence. Sci. Rep. **5**, 14004 (2015)
30. C.W. Lai, J. An, H.C. Ong, Surface-plasmon-mediated emission from metal-capped ZnO thin films. Appl. Phys. Lett. **86**, 251105 (2005)
31. R.J.V. Michael, B. Sambandam, T. Muthukumar, M.J. Umapathy, P.T. Manoharan, Spectroscopic dimensions of silver nanoparticles and clusters in ZnO matrix and their role in bioinspired antifouling and photocatalysis. Phys. Chem. Chem. Phys. **16**, 8511–8555 (2014)
32. S.K. Evstropiev, N.V. Nikonorov, A.S. Saratovskii, Double stabilization of silver molecular clusters in thin films. Res. Chem. Intermed. **46**, 4033–4046 (2020). https://doi.org/10.1007/s11164-020-04189-6
33. S.K. Evstropiev, N.V. Nikonorov, A.S. Saratovskii, K.V. Dukelskii, V.N. Vasiliev, A.V. Karavaeva, I.P. Soshnikov, Photo-stimulated evolution of different structural forms of silver in solutions, composite and oxide coatings. J. Photochem. Photobiol. A: Photochem. **403**, 112858 (2020). https://doi.org/10.1016/j.jphotochem.2020.112858
34. C. Karunakaran, V. Rajeswari, P. Gomathisankar, Enhanced photocatalytic and antibacterial activities of sol-gel synthesized ZnO and Ag-ZnO. Mater. Sci. Semicond. Process. **14**, 133–138 (2011)
35. H.B. Dias, M.I.B. Bernardi, V.S. Marangoni, A.C. de Abreu Bernardi, A.N. de Souza Rastelli, A.C. Hernandes, Synthesis, characterization and application of Ag doped ZnO nanoparticles in a composite resin. Mater. Sci. Eng.: C **96**, 391–401 (2019)
36. T. Siva Vijayakumar, S. Karthikeyeni, S. Vasanth, A. Ganesh, G. Bubesh, R. Ramesh, M. Manimegaeai, P. Subramanian, Synthesis of silver-doped zinc oxide nanocomposite by pulse mode ultrasonication and its characterization studies. J. Nanosci. **2013**, 1–7 (2013). https://doi.org/10.1155/2013/785064
37. J. Wang, Y. Liu, Y. Jiao, F. Qu, Q. Pan, X. Wu, Hybrid Ag_2O/ZnO heterostructures. J. Nanomater. **2013**, 1–5 (2013). https://doi.org/10.1155/2013/684797
38. M.J. Height, S.E. Pratsinis, O. Mekasuwandumrong, P. Praserthdam, Ag-ZnO catalysts for UV-photodegradation of methylene blue. Appl. Catal. B: Environ. **63**, 305–312 (2006)
39. T. Chitradevi, A. Jestin Lenus, N. Victor Jaya, Structure, morphology and luminescence properties of sol-gel method synthesized pure and Ag-doped ZnO nanoparticles. Mater. Res. Express **7**, 015011 (2020)
40. B.D. Ahn, H.S. Kang, J.H. Kim, G.H. Kim, H.W. Chang, S.Y. Lee, Synthesis and analysis of Ag-doped ZnO. J. Appl. Phys. **100**, 093701 (2006). https://doi.org/10.1063/1.2364041
41. R. Sánchez Zeferino, M. Barboza Flores, U. Pal, Photoluminescence and Raman scattering in Ag-doped ZnO nanoparticles. J. Appl. Phys. **109**, 014308 (2011)
42. I.G. Tredici, A. Resmini, S. Pin, P. Chigna, T. Rovetta, M. Patrini, N. Rotiroti, M. Dapiaggi, U. Anselmi-Tamburini, Mechanisms of zinc oxide nanocrystalline thin film formation by thermal degradation of metal-loaded hydrogels. J. Phys. Chem. C **117**, 25108–25117 (2013)
43. T.J.B. Holland, S.A.T. Redfern, Unit cell refinement from powder diffraction data: the use of regression diagnostics. Miner. Mag. **61**, 65–77 (1997)
44. Z. Huang, X. Zheng, D. Yan, G. Yin, X. Liao, Y. Kang, Y. Yao, D. Huang, B. Hao, Toxicological effect of ZnO nanoparticles based on bacteria. Langmuir **24**, 4140–4144 (2008)
45. P. Warneck, C. Wurzinger, Product quantum yields for the 305-nm photodecomposition of NO_3^- in aqueous solution. J. Phys. Chem. **92**, 6278–6283 (1988)
46. B.A. Ashenfelter, A. Desireddy, H.Y. Sung, T. Goodson III., T.P. Bigioni, Fluorescence from molecular silver nanoparticles. J. Phys. Chem. C **119**, 20728–20734 (2015)
47. M. Van der Linden, A. Barendregt, A.J. van Bunningen, P.T.K. Chin, D. Thies-Weesie, F.M.F. de Groot, A. Meijerink, Characterization, degradation and regeneration of luminescent Ag_{29} clusters in solution. Nanoscale **8**, 19901–19909 (2016)
48. S. Lecoultre, A. Rydlo, J. Buttet, C. Félix, S. Gilb, W. Harbich, Ultraviolet-visible absorption of small silver clusters in neon: Ag_n (n=1-9). J. Chem. Phys. **134**, 184504 (2011)
49. M. Harb, F. Rabilloud, D. Simon, A. Rydlo, S. Lecoultre, F. Conus, V. Rodrigues, C. Félix, Optical absorption of small silver clusters: Ag_n, (n=4-22). J. Chem. Phys. **129**, 194108 (2008). https://doi.org/10.1063/1.3013557
50. M.V. Stolyarchuk, A.I. Sidorov, Electronic absorption spectra of neutral and charged silver molecular clusters. Opt. Spectrosc. **125**, 305–310 (2018)
51. P.Y. Silvert, R. Herrera-Urbina, K. Tekaia-Elhsissen, Preparation of colloidal silver dispersions by the polyol process. Part. 2 – Mechanism of particle formation. J. Mater. Chem. **7**, 293–299 (1997)
52. H. Wang, X. Qiao, J. Chen, X. Wang, S. Ding, Mechanism of PVP in the preparation of silver nanoparticles. Mater. Chem. Phys. **94**, 419–453 (2005)
53. C. Kan, W. Cai, C. Li, L. Zhang, Optical studies of polyvinylpyrrolidone reduction effect on free and complex metal ions. J. Mater. Res. **20**, 320–324 (2005)
54. G.A. Ozin, H. Huber, Cryophotoclustering techniques for synthesizing very small, naked silver clusters Ag_n of known size (where

n=2-5). The molecular metal cluster-bulk metal particle interface. Inorg. Chem. **17**, 155–163 (1978)
55. M.M. Obeid, H.R. Jappor, K. Al-Marzoki, I.A. Al-Hydary, S.J. Edrees, M.M. Shukur, Unraveling the effect of Gd doping on the structural, optical, and magnetic properties of ZnO diluted magnetic semiconductor nanorods. RSC Adv. **9**, 33207–33221 (2019)
56. J.P. Wang, Z.Y. Wang, B.B. Huang, Y.D. Ma, Y.Y. Liu, X.Y. Zhang, Y. Dai, Oxygen vacancy induced band gap narrowing and enhanced visible light photocatalytic activity of ZnO. ACS Appl. Mater. Interfaces **4**, 4024–4030 (2012)
57. X.H. Lu, G.M. Wang, S.L. Xie, J.Y. Shi, W. Li, Y.X. Tong, Y. Li, Efficient photocatalytic hydrogen evolution over hydrogenated ZnO nanorod arrays. Chem. Commun. **48**, 7717–7719 (2012)
58. D.M. Hofmann, D. Pfisterer, J. Sann, B.K. Meyer, R. Tena-Zaera, V. Munoz-Sanjose, T. Frank, G. Pensl, Properties of the oxygen vacancy in ZnO. Appl. Phys. A **88**, 147–151 (2007)